Quantum Effects on Hydrogen Adsorption in Internal Nanospaces of Single-Wall Carbon Nanohorns

Hideki Tanaka,*,† Hirofumi Kanoh,‡ Mustapha El-Merraoui,‡ William Arthur Steele,§ Masako Yudasaka,†,|| Sumio Iijima,†,||,⊥ and Katsumi Kaneko‡

SORST, Japan Science and Technology Agency, c/o NEC Corporation, 34 Miyukigaoka, Tsukuba 305-8501, Japan, Department of Chemistry, Faculty of Science, Chiba University, 1-33 Yayoi, Inage, Chiba 263-8522, Japan, Department of Chemistry, NEC Corporation, 34 Miyukigaoka, Tsukuba 305-8501, Japan, 152 Davey Laboratory, Pennsylvania State University, University Park, Pennsylvania 16802, and Department of Physics, Meijo University, 1-501 Shiogamaguchi, Tenpaku, Nagoya 468-8502, Japan

Received: March 31, 2004; In Final Form: August 25, 2004

Hydrogen adsorption isotherms in single-wall carbon nanohorns (SWNHs) have been measured at 20 K. The pore volume from hydrogen adsorption is compared with that from nitrogen adsorption at 77 K to determine the density of confined hydrogen in the internal space of SWNHs; it indicates that the average density of confined hydrogen inside SWNHs at 20 K is higher than that of liquid hydrogen in the bulk and nearly approaches the density of solid hydrogen at the triple point. The surface area from hydrogen adsorption using the BET theory is anomalously large compared with that for nitrogen; however, an alternative method (modified BET theory), in which an assumption is made that the energy of a molecule in the second layer is larger than that in the liquid, gives a reasonable surface area, especially when the adsorbed hydrogen in the first layer is assumed to be in a solid state. In the modified BET model, a packing constraint of the second layer due to the cylindrical geometry of SWNH is also taken into account. The solidlike behaviors of adsorbed hydrogen would be attributed to quantum effects, which give a strongly attractive pore situation for the hydrogen−SWNH system.

Introduction

Hydrogen adsorption in a porous medium at low temperature has received considerable attention in recent decades[1−6] because quantum liquid hydrogen has large zero point energy compared with the binding energy, and thus, it might be strongly affected by confinement in a small pore due to the weak intermolecular interaction. The character of hydrogen confined in Vycor glass with cylindrical nanoscale pores has been the subject of several studies[1−3] because the confinement in mesopores of Vycor glass may offer the possibility of observing superfluid behavior of hydrogen. Ginzberg and Sobyanin[7] suggested that liquid hydrogen would transition to Bose condensed phase at 6 K in the absence of intermolecular interactions. However, this transition is preempted by solidification of hydrogen at 13.8 K in the bulk, and thus, the confinement of liquid hydrogen in Vycor glass has attracted attention because it has been known for a long time that the liquid−solid transition temperature is usually depressed when a liquid is confined in small pores. Torii and co-workers[2] performed a comprehensive study for the phase diagram of hydrogen confined in Vycor glasses using the heat capacity measurements. They reported that suppressed freezing transitions of confined hydrogen occur at about 9 and 12 K for large-pore samples (diameter: $d = 3-6$ nm) and that no liquid−solid transition is observed for small-pore samples ($d \approx 2$ nm); however, superfluid transition of hydrogen is not detected. Sokol and co-workers[3] have investigated the structure of confined hydrogen in Vycor glass using the neutron scattering measurement. Their study showed that the confined hydrogen can be described as a bulklike liquid at temperatures above 12 K, and on cooling, a solid phase is formed at 10 K with a structure unlike that of the bulk solid. From these studies mentioned above, the confined hydrogen in Vycor glasses has been believed to be a bulklike liquid above ca. 12 K; however, in contrast, Edler and co-workers[8] suggested that the confined hydrogen in the mesopores of MCM-41, which is a siliceous material with a regular array of hexagonal and unidimensional mesopores, behaves like a solid rather than a liquid at 21.5 K. They measured nitrogen and hydrogen adsorption isotherms on MCM-41 ($d \approx 3.5$ nm) at 77 and 21.5 K, respectively, and compared the mesopore volume and the BET surface area that were obtained from the hydrogen isotherm with those obtained from the nitrogen isotherm. The mesopore volume that was calculated from the adsorbed amount at the relative pressure of 0.95 by assuming that the mesopores have been filled with liquid hydrogen was 21% larger than the value from the nitrogen isotherm. However, by calculating the mesopore volume using the density of solid hydrogen, the agreement with the nitrogen data was better (11% smaller than the value from the nitrogen adsorption). The surface area from the hydrogen isotherm was obtained by multiplying the BET monolayer capacity by the cross-sectional area of a hydrogen molecule, which was calculated from the bulk liquid density by assuming the close packing of spheres, whereas for nitrogen, the cross-sectional area was 0.162 nm^2. The value of the surface area from the hydrogen isotherm was 40% larger than that from the nitrogen isotherm; however, by calculating the cross-sectional area of

* Corresponding author. Present address: Diversity and Fractal Science, Graduate School of Science and Technology, Chiba University, 1-33 Yayoi, Inage, Chiba 263-8522, Japan. Tel: +81-43-290-3940. Fax: +81-43-290-2788. E-mail: tanaka@pchem2.s.chiba-u.ac.jp.

† SORST.

‡ Chiba University.

§ Pennsylvania State University.

|| NEC Corporation.

⊥ Meijo University.

10.1021/jp048603a CCC: $27.50
Published on Web 10/15/2004

hydrogen using the density of solid hydrogen, a better agreement was obtained (14% larger than the value from the nitrogen adsorption). They also confirmed the solidlike hydrogen in the mesopores of MCM-41 using the neutron scattering experiments. This may indicate that a freezing point elevation of confined hydrogen occurs in the mesopores of MCM-41. Moreover, Miyahara and Gubbins[9] predicted a freezing point elevation (over the boiling point in the bulk) of adsorbed Lennard-Jones (LJ) methane in carbon slit pores using grand canonical Monte Carlo (GCMC) simulations, and Watanabe et al. experimentally observed the elevation in freezing temperature for benzene confined in graphitic slit pores by differential scanning calorimetry (DSC) measurements.[10] Maddox and Gubbins[11] extended the work by Miyahara and Gubbins to multiwall carbon nanotubes with inner diameters in the rage of 1.5−3.5 nm, showing that the fluid−wall interactions, which are relatively stronger than the fluid−fluid interaction, cause the freezing point elevation in adsorbed layers near the wall. Therefore, if hydrogen is confined in carbon mesopores, which have more strongly attractive fluid−wall interactions than MCM-41, then we should observe a solidlike phase of confined hydrogen rather than liquidlike phase. An additional point this requirement is that carbon-nanotube-related materials are interesting porous mediums because they must have strong fluid−wall interactions due to the high density of carbon atoms in the walls compared with siliceous material, such as MCM-41 and Vycor glass. Moreover, recent molecular simulations and a theoretical calculation including quantum effects have been performed to determine hydrogen adsorption in single-wall carbon nanotubes (SWNTs) at low temperature and to give an indication of the importance of quantum effects for hydrogen adsorption.[12−18] Therefore, it is of great interest to study hydrogen adsorption on SWNT related materials experimentally.

Recently, Harris et al.[19] and Iijima et al.[20] discovered single-wall carbon nanohorns (SWNH) of which fundamental tube structure is similar to that of SWNTs. Iijima et al. reported that sufficient amounts of SWNHs with a high purity (>90%) can be produced by a CO_2 laser ablation of pure graphite in an atmospheric pressure of argon gas without any metal catalysts at room temperature.[20] A SWNH has a typical tube diameter of about 3 nm with length in the range of 40−50 nm and a cone cap at the one end of the tube. SWNHs are associated each other to form a *Dahlia* flowerlike assembly structure (diameter: 80−100 nm), providing nanoporosity.[21−26] Because abundant SWNHs of several grams with high yield and purity are easily produced, a systematic study on physical adsorption for SWNHs can be carried out; thus, it will also lead to a clear understanding of the physical adsorption of hydrogen for SWNT-related materials.

Experimental Section

An as-grown SWNH sample was oxidized to open nanoscale windows on the wall of the SWNH particle at 693 K (denoted as as-SWNH and ox-SWNH, respectively). Details of the oxidation method have been provided elsewhere.[22] The adsorption isotherms of hydrogen at 20 K and nitrogen at 77 K for the SWNH samples were measured with laboratory-designed volumetric adsorption equipment. The apparatus consists of a gas handling system and a cryostat with a He closed-cycle refrigerator. All samples were outgassed under a vacuum greater than 0.1 mPa at 423 K for 2 h. The temperature was kept within ±0.05 K during the adsorption measurement. Thermal transpiration was corrected by the use of the empirical equation of Takaishi and Sensui.[27]

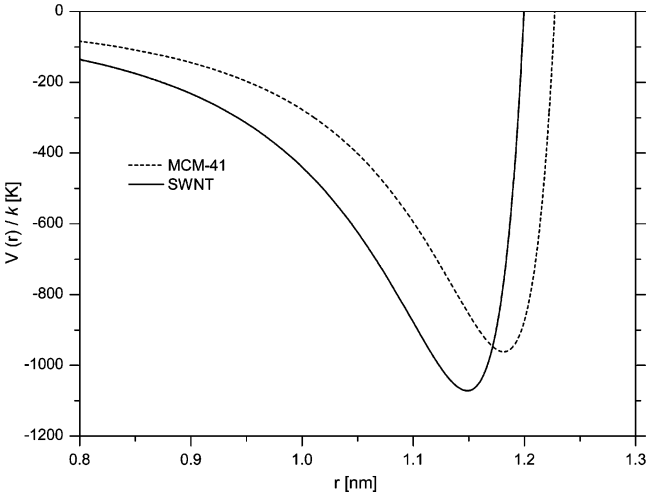

Figure 1. The solid-fluid interaction potentials for nitrogen inside MCM-41 (- - -) and SWNT (—) with $D = 3.0$ nm.

Potential Models and Theoretical Approaches

Molecular Potential and Quantum Contribution. The Lennard-Jones (LJ) potential was used to model solid−fluid interactions. For simplicity, we assumed a homogeneous cylindrical tube like SWNT. The fluid−wall interaction inside SWNT can be calculated using the LJ potential integrated over an infinitely long cylinder[28,29]

$$V(r, R) = \pi^2 \rho_s \epsilon_{sf} \sigma_{sf}^2 \left[\frac{63}{32} \frac{F(-4.5, -4.5, 1.0; \beta^2)}{[R^*(1-\beta^2)]^{10}} - 3\frac{F(-1.5, -1.5, 1.0; \beta^2)}{[R^*(1-\beta^2)]^4} \right]$$

$$\beta = \frac{r}{R} \qquad R^* = \frac{R}{\sigma_{sf}} \tag{1}$$

where $F(\alpha, \beta, \gamma ; \chi)$ is a hypergeometric function, R and ρ_s are the radius of the tube and density of solid atoms in the tube wall (in the case of SWNT, $\rho_s = 38.2$ nm^{-2}), respectively. The interaction parameters for the model SWNT are $\sigma_{sf} = 0.3494$ nm and $\epsilon_{sf}/k = 53.22$ K for nitrogen and $\sigma_{sf} = 0.3179$ nm and $\epsilon_{sf}/k = 32.06$ K for hydrogen, respectively. Ravikovitch and co-workers[30] suggested that this integrated LJ potential model well describes nitrogen adsorption behaviors in the mesopores of MCM-41 by assuming that the mesopores are composed of oxygen atoms (the parameters are $\sigma_{sf} = 0.317$ nm and $\rho_s\epsilon_{sf}/k = 2253$ K/nm^2). The fluid−wall interaction potentials for nitrogen inside the model SWNT and MCM-41 with the same pore diameter ($D = 3$ nm: internuclear distance) are shown in Figure 1. The magnitude of the potential energy minimum for SWNT (1074 K) is larger than that for MCM-41 (966 K). This indicates that the interior of SWNT (and also the tubular part of SWNH) has a more attractive fluid−wall interaction potential than MCM-41 and that this would be basically the same in the case of hydrogen.

We consider here quantum contributions for the fluid−wall and fluid−fluid interaction potentials for hydrogen. The Feynman's procedure, which employs an "effective potential" given by eq 2, can be applied to evaluate the quantum effects[4,31]

$$V_{eff}(\mathbf{r}) = \left(\frac{\sqrt{3}}{l\sqrt{\pi}}\right)^3 \int d\mathbf{r}'\, V(\mathbf{r}') \exp\left[\frac{-3(|\mathbf{r}-\mathbf{r}'|)^2}{l^2}\right] \tag{2}$$

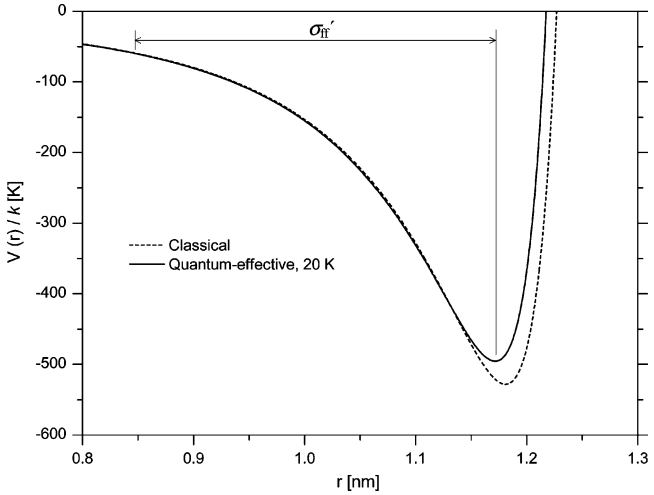

Figure 2. The solid−fluid interaction potentials for hydrogen inside SWNT with $D = 3.0$ nm. The dashed and solid lines represent the classical potential and quantum effective potential at 20 K, respectively.

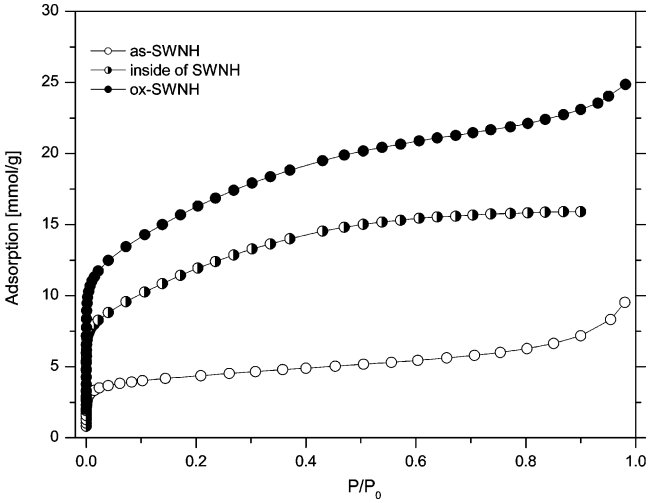

Figure 3. Nitrogen adsorption isotherms for as-SWNH, ox-SWNH, and the internal space of SWNHs at 77 K.

where $l^2 = \hbar^2/(6mkT)$ and m is the molecular mass of hydrogen. This effective potential represents a smearing of the classical potential (e.g., eq 1) as a first quantum correction. Figure 2 represents the fluid−wall interaction potential for classical (LJ) hydrogen inside SWNT with a diameter of 3 nm calculated by eq 1 and the effective potential for quantum (LJ) hydrogen using eq 2 with eq 1 at 20 K. The potential well depth of SWNT for quantum hydrogen is reduced by 32 K (6%) compared with that for classical hydrogen because of the quantum effects. According to Young,[32] when a classical fluid−fluid interaction is represented by the LJ pair interaction potential, $V_{LJ}(|\mathbf{r} - \mathbf{r}'|)$, the quantum effects are included by replacing parameters ϵ_{ff} and σ_{ff} in V_{LJ} with temperature- and λ-dependent parameters ϵ_{ff}' and σ_{ff}' (where $\lambda = h/\sigma_{ff}(m\epsilon_{ff})^{1/2}$). The parameters ϵ_{ff}' and σ_{ff}' can be estimated by Feynman's effective potential[31] method. For quantum hydrogen pairs, the location of the minimum of the effective potential is shifted to $2^{1/6}\sigma_{ff}'$ and the potential well depth, to $-\epsilon_{ff}'$. The quantum contributions are $\sigma_{ff}'/\sigma_{ff} = 1.094$ and $\epsilon_{ff}'/\epsilon_{ff} = 0.614$ at 20 K ($\sigma_{ff} = 0.2985$ nm and $\epsilon_{ff}/k = 36.7$ K were used), respectively. The fluid−fluid interaction potential well depth of quantum hydrogen at 20 K is 39% smaller than that of classical hydrogen; thus, this indicates that the difference between the fluid−wall and fluid−fluid interactions becomes significant because of the quantum effects at 20 K.

Density Functional Theory (DFT). DFT is a powerful tool for descriptions of confined systems of classical fluids in mesopores.[30,33] Additionally, the DFT calculations are not time consuming, and thermodynamic equilibrium capillary condensation can be easily determined in compared with the GCMC simulations. The DFT method is based on the idea that the grand thermodynamic potential of confined fluids can be reproduced by a functional of the local fluid density $\rho(\mathbf{r})$. The basic formulations for the DFT calculations can be found in ref 34.

In the present study, nitrogen adsorption isotherms inside model SWNTs were calculated by Tarazona's version of the nonlocal density functional theory.[35] In the DFT approach, the attractive part of the fluid−fluid interaction is modeled with the LJ potential, split at its minimum, $r_m = 2^{1/6}\sigma_{ff}$, according to the Weeks−Chandler−Andersen prescription[36] and the repulsive part of the fluid−fluid interaction is modeled by an equivalent hard-sphere potential with an appropriate hard-sphere diameter d_{hs}. The cutoff distance of the LJ potential, r_c, was set to 5 σ_{ff}. We chose $\sigma_{ff} = 0.3575$ nm, $\epsilon_{ff}/k = 94.45$ K, and $d_{hs} = 0.3575$ nm as the fluid−fluid interaction parameters modeling nitrogen, which have been proposed by Ravikovitch and coworkers.[30,37] They determined the parameters so that the theory could reproduce the experimental liquid−gas coexisting densities, saturation pressure, and surface tension of the liquid−gas interface of nitrogen at the normal boiling temperature and obtained good agreement between the DFT and GCMC nitrogen adsorption isotherms.

In this study, the results from the DFT models will be discussed in the form of the excess adsorption per unit pore volume, Γ_v. The Γ_v value inside SWNT was calculated from the radially symmetric local density profile of adsorbed phase, $\rho(r)$

$$\Gamma_v = \frac{2}{(R - \sigma_{ss}/2)^2}\int_0^{R-\sigma_{ss}/2} r\{\rho(r) - \rho_b\}dr \qquad (3)$$

where R, σ_{ss} (= 0.34 nm), and ρ_b are the radius of the model SWNT, the size parameter of carbon atom in the wall of SWNT, and the density of the bulk gas phase at the same adsorption temperature and pressure, respectively.

Results and Discussion

Nitrogen Adsorption Isotherms on SWNHs and Comparison with the DFT Models. Figure 3 shows nitrogen adsorption isotherms on as-SWNH and ox-SWNH at 77 K, where the adsorption isotherm of nitrogen inside SWNHs is also shown. The adsorption isotherm for the internal space of SWNHs was obtained by subtraction of the isotherm on as-SWNH from that on ox-SWNH. Theoretical adsorption isotherms calculated by the DFT models with a tube diameter of $D = 2$, 3, 4.5, and 6 nm are presented in Figure 4a and b, together with the experimental isotherm of nitrogen inside SWNHs. The experimental data for the interior space of SWNHs was divided by the pore volume (0.55 cm^3/g, Table 1) calculated by using the bulk liquid density (28.9 $mmol/cm^3$) to compare with the theoretical isotherms. The DFT adsorption isotherms have a steplike behavior below $P/P_0 = 10^{-3}$, indicating the monolayer completion on the internal wall of the model SWNTs (Figure 4a). In contrast with the DFT models, the experimental isotherm inside SWNH exhibits a gradual step over the P/P_0 range of 10^{-5}−10^{-3}. The pressure of the monolayer completion inside the model SWNT ($D = 2$ nm) is close to the beginning of the gradual step for SWNH, although the nitrogen filling in the cone part of SWNH that the diameter of the base is 2 nm,

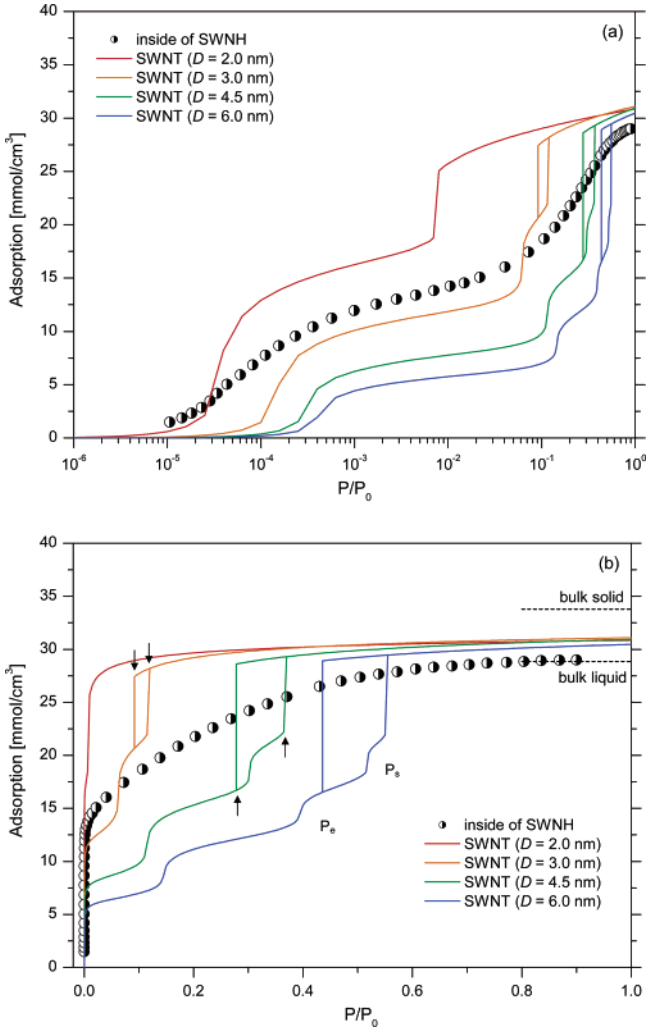

Figure 4. Nitrogen adsorption isotherms at 77 K. The circles represent the experimental values for the internal space of SWNHs. The four lines are predictions from the DFT calculations for the inside of the model SWNTs (D = 2.0, 3.0, 4.5, and 6.0 nm). The arrows denote the positions of the spontaneous capillary condensation (right) and the equilibrium transition (left), respectively. The relative pressures are given in (a) logarithmic and (b) linear scales. The dashed lines represent the bulk liquid and solid densities at the boiling and triple points.

TABLE 1: BET Surface Areas for the Interior of SWNHs

N_2 (77 K)			H_2 (20 K)			
n_m[a] mmol/g	S_{BET}[b] m^2/g	P/P_0[c]	n_m[a] mmol/g	S_{BET}[b] m^2/g	P/P_0[c]	Δ[d] %
9.6	938[(l)e]	0.02−0.27	15.7	1353[(l)e]	0.02−0.15	44
				1179[(s)e]		26

[a] n_m denotes BET monolayer capacity. [b] S_{BET} denotes BET surface area. [c] P/P_0 refers to the range of least-squares fitting for BET analysis. [d] Δ denotes the difference from the surface area obtained by nitrogen adsorption. [e] (l)(s) refer to surface areas estimated by use of the cross-sectional areas, which were calculated from the bulk liquid and solid (triple point) densities by assuming the close packing of spheres.

should occur at a lower relative pressure than the DFT model due to strong fluid−wall interaction potential in the cone part. This indicates that the adsorption amount of nitrogen in the cone part of SWNH is fairly small; thus, the gradual step (P/P_0 = 10^{-5}−10^{-3}) is attributed to the size distribution of the tubular part of SWNH. Here, we assume that SWNH is composed of a cylindrical tube (length: l_1, diameter: D) and a cone (length: l_2, diameter of the base: D) part. The volume ratio of the cone part to the total volume of SWNH can be calculated by $l_2/(3l_1 + l_2)$ and is smaller than 6%, when the D value is 2 nm, and the lengths are $l_2 \approx 6$ nm, and $l_1 + l_2 = 40$ nm, respectively (these values should be reasonable from TEM observations[20]). Therefore, the adsorption in the cone part, where the diameter of the base is smaller than 2 nm, does not strongly affect the nitrogen adsorption isotherm inside the SWNHs.

Hysteresis loops on the DFT isotherms ($D \geq 3$ nm) correspond to spontaneous capillary condensation (vaporlike spinodal) and equilibrium (desorption) transition ($P/P_0 = P_s$ and P_e, Figure 4b). The thermodynamic grand potentials on the adsorption and desorption branches are the same at the equilibrium transition ($P/P_0 = P_e$). However, the adsorption hysteresis is not clearly observed for the experimental adsorption isotherm inside SWNHs (not shown). Two possible reasons may be considered; the first one is that a vaporlike spinodal on the adsorption process cannot be achieved on the inside of SWNHs, that is, SWNH can be regarded as a close-ended pore system with no influence of the nanoscale windows on the wall of SWNH, and the adsorption proceeds through the thermodynamically stable sate ($P/P_0 = P_e$). In the DFT model, it corresponds to an open-ended pore system because the infinitely long tube model is used, thus, the vaporlike spinodal is observed for the adsorption branch. The second one is that the hysteresis loop cannot be detected experimentally due to the gradual increase (decrease) of the adsorption (desorption) isotherm in the region of the capillary condensation. In any case, we discuss using the equilibrium transition branch of the DFT model because the experimental adsorption branch should be regarded as the same with the desorption branch and as the equilibrium state within experimental errors.

The experimental adsorption isotherm inside SWNHs shows a gradual increase over the relative pressure range of 0.01−0.5, and it can be related to the multilayer adsorption and capillary condensation inside SWNHs ($D \geq 2$ nm) by comparing it with the DFT models (Figure 4b). Moreover, the nitrogen isotherm inside the SWNHs has a definite plateau over ca. P/P_0 = 0.5; thus, it indicates that the tube size distribution of SWNHs ranges to 6 nm.

Average Density of Confined Nitrogen. In the present study, we used the nitrogen adsorption at $P/P_0 = 0.8$ to calculate the pore volume of SWNHs because the adsorption isotherm inside the SWNHs can be affected by a difference in interparticle condensation behaviors between as-SWNH and ox-SWNH above $P/P_0 = 0.8$ (Figure 3), although the adsorbed amount at $P/P_0 = 0.95$ is usually used. At $P/P_0 = 0.8$, average densities of confined nitrogen from the DFT models are 4.4−7.1% larger than that of liquid nitrogen in the bulk at the normal boiling temperature. This indicates that the pore volume inside SWNHs can be evaluated using the bulk liquid density within ca. 7% deviation.

The structures of adsorbed nitrogen inside the SWNTs should be different from that in the bulk because of the confinement, even though the average densities of confined nitrogen are almost the same with liquid nitrogen. Figure 5a−d show local density profiles of confined nitrogen from the DFT models at $P/P_0 = 0.8$. The local density profiles from all the DFT models exhibit two highly pronounced peaks starting from the pore wall, corresponding to the contact and second layers of nitrogen. The peaks with large local densities suggest that the adsorbed layers near the pore walls are structured compared with those of the bulk liquid. This coincides with preceding experimental facts that molecules confined in slit shaped carbon micropores form highly organized structures.[38−41] The structure of the condensate in the central region of the SWNTs is strongly affected by the

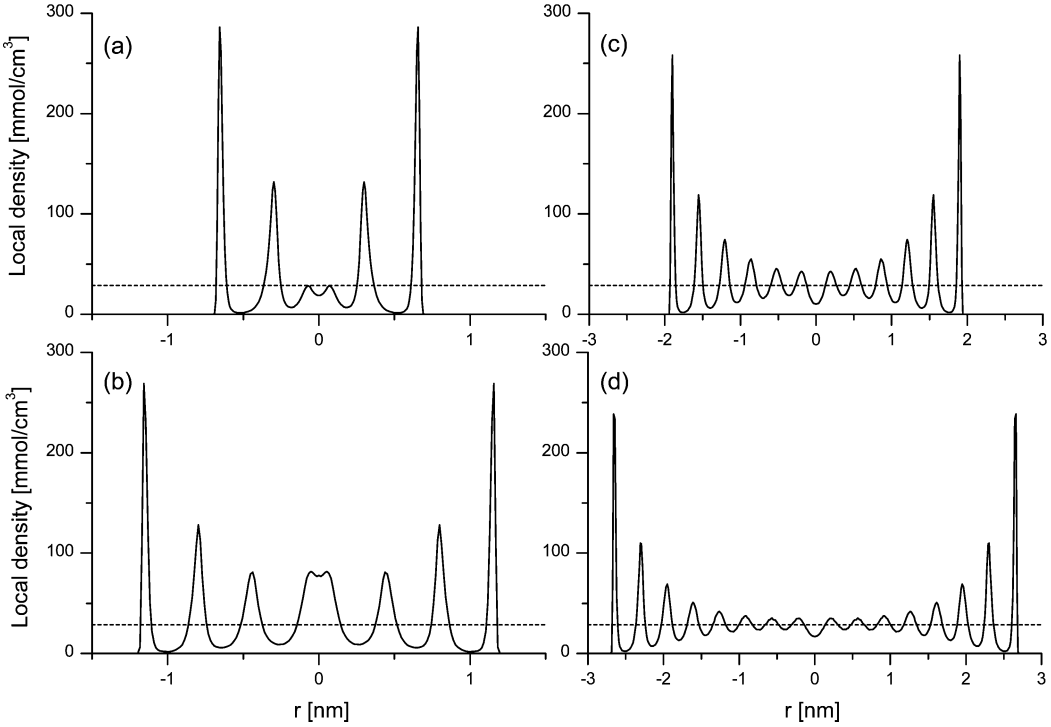

Figure 5. Local density profiles of nitrogen inside SWNTs from DFT at $P/P_0 = 0.8$ and 77 K. (a) $D = 2.0$ nm, (b) $D = 3.0$ nm, (c) $D = 4.5$ nm, and (d) $D = 6.0$ nm. The dashed line represents the bulk liquid density.

tube diameter. The DFT model ($D = 2$ nm) shows third layers with smaller local density than that of the bulk liquid due to the geometrical constraint of the cylindrical pore. However, for $D = 3$ nm, highly structured third and forth layers are observed, and then the structuring becomes weak by layer by layer because of the decrease in the fluid−wall interactions for larger pores ($D = 4.5-6$ nm). Thus, the local density profile in the central region of SWNT that is larger than 6 nm in diameter should be close to the average density of the bulk liquid. These facts suggest that condensates inside SWNHs have different local densities from the bulk liquid nitrogen depending on the tube diameter and the location in the internal of SWNHs, although the average density of confined nitrogen inside SWNHs should be almost identical with that of the bulk liquid.

Monolayer Density of Adsorbed Nitrogen. We have obtained 2D monolayer density of nitrogen, Γ_m, from the DFT model by

$$\Gamma_m = \frac{1}{R - \sigma_{ss}/2}\int_a^R r\rho(r)\,dr \qquad (4)$$

where $a = R - \sigma_{sf} - \sigma_{ff}/2$. The Γ_m value represents the number of moles of nitrogen per internal surface area of SWNT. Calculated monolayer densities are shown in Figure 6a and b as a function of relative pressure, together with the density (dashed line), $\rho_{2D-bulk}$, obtained from the cross-sectional area of nitrogen (0.162 nm^2), which is usually used to evaluate the BET surface area. All of the DFT models predict smaller monolayer density than the value of $\rho_{2D-bulk}$ over the relative pressure range of 0.05−0.35, where the BET equation is conventionally applied. This suggests that the use of the cross-sectional area of nitrogen of 0.162 nm^2 results in underestimating the surface area of SWNT (especially for small SWNTs), even if the correct monolayer capacity is obtained by fitting the BET equation. The difficulty in determining precise surface areas of cylindrical pores using the BET method has been already pointed

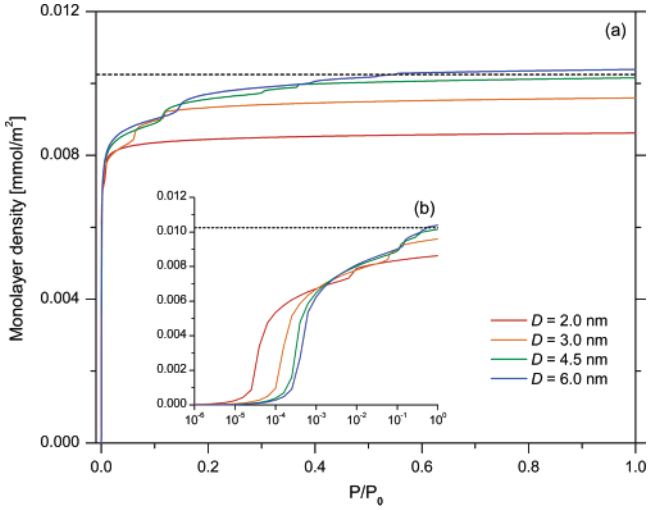

Figure 6. Monolayer densities of nitrogen per internal surface areas of SWNTs ($D = 2.0$, 3.0, 4.5, and 6.0 nm) by DFT at 77 K as a function of pressure. The relative pressures are given in (a) linear and (b) logarithmic scales, respectively. The dashed line represents the two-dimensional density of nitrogen calculated by the cross-sectional area of 0.162 nm^2.

out by Ohba and Kaneko using GCMC simulations.[43] Note that the monolayer capacity obtained by the BET plot should tend to be overestimated in the case of the inside of SWNHs. This is because SWNHs with a diameter smaller than ca. 4.5 nm should be perfectly filled by nitrogen, and second layer adsorption can occur for larger SWNHs below $P/P_0 = 0.27$ (Figure 4b). Therefore, unfortunately, the BET surface area from the nitrogen adsorption inside SWNHs would be strongly affected by both the underestimation of the cross-sectional area of a nitrogen molecule and the overestimation of the monolayer capacity due to multilayer adsorption and capillary condensation, whereas the fitting of the nitrogen adsorption isotherm inside SWNHs to the BET equation gives a good agreement over the range of $P/P_0 = 0.02-0.27$. The monolayer density per internal

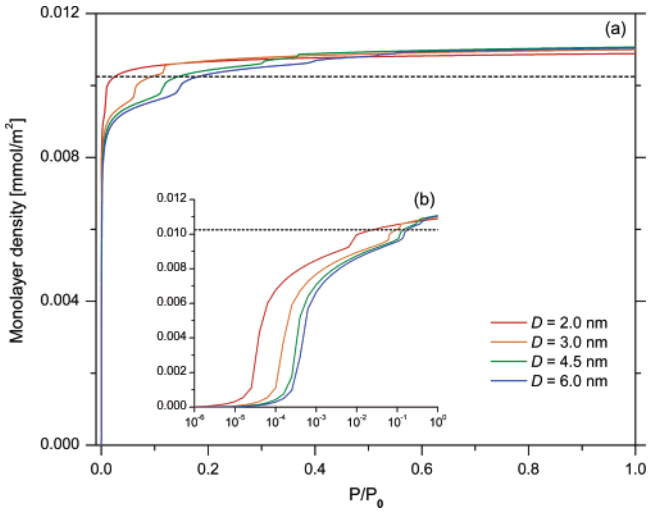

Figure 7. Monolayer densities of nitrogen inside SWNTs (D = 2.0, 3.0, 4.5, and 6.0 nm) from DFT at 77 K as a function of pressure. The relative pressures are given in (a) linear and (b) logarithmic scales, respectively. The dashed line represents the 2D density of nitrogen calculated by the cross-sectional area of 0.162 nm^2.

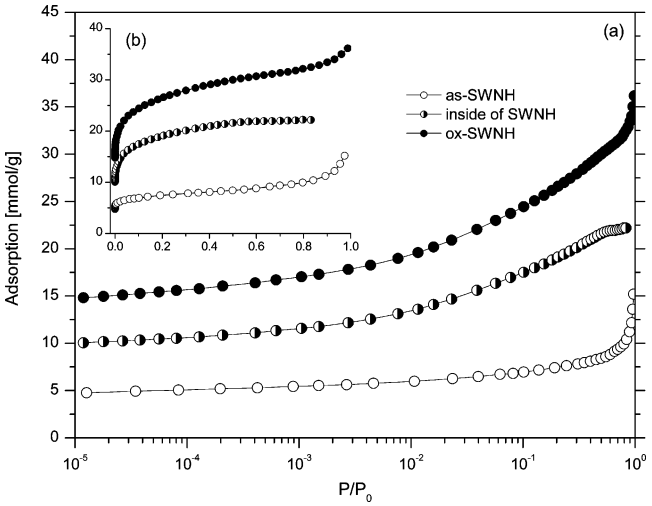

Figure 8. Experimental hydrogen adsorption isotherms for as-SWNH, ox-SWNH, and the internal space of SWNHs at 20 K. The relative pressures are given in (a) logarithmic and (b) linear scales, respectively.

surface area of SWNT tends to be lower than the $\rho_{2D-bulk}$ value because the radius of the cylindrical monolayer film is smaller than that of the carbon surface. Note that the monolayer density of the adsorbed nitrogen from the DFT model is actually close to the $\rho_{2D-bulk}$ value in the intermediate relative pressure region, if the density of the first layer can be defined as

$$\Gamma'_m = \frac{1}{R_m}\int_a^R r\rho(r)\,dr \qquad (5)$$

where R_m is the radius of the cylindrical first layer film, at which the local density of the monolayer shows a maximum. The Γ'_m values calculated for the respective SWNT models are shown in Figure 7a and b as a function of relative pressure. The results suggest that the average density of the adsorbed nitrogen in the first layer on the internal surface of SWNT ($D \geq 2$ nm) is in agreement with $\rho_{2D-bulk}$ within approximately 8% deviation over the relative pressure of 0.05−1.

Adsorption Isotherms of Quantum Hydrogen on SWNHs. Figure 8 shows hydrogen adsorption isotherms on as-SWNH and ox-SWNH at 20 K. The adsorption isotherm in the internal space of SWNHs was obtained by subtracting the adsorption isotherm on as-SWNH from that on ox-SWNH and is also shown in Figure 8. The adsorption isotherm of hydrogen inside SWNHs exhibits significant uptake at low relative pressures. This is to be expected from that the adsorption isotherm of hydrogen on a graphite basal plane from path integral Monte Carlo (PIMC) simulations showing a monolayer formation around $P/P_0 = 10^{-9}$ at 20 K;[42] thus, the monolayer formation on the internal wall of SWNHs should occur below $P/P_0 = 10^{-9}$ because of large fluid−wall interactions inside SWNHs ($D < \sim 3$ nm) compared with that on the graphite basal plane.

Monolayer Density of Adsorbed Quantum Hydrogen. The surface areas were calculated by multiplying the BET monolayer capacity from the hydrogen adsorption isotherm inside SWNHs by the cross-sectional areas (0.143 and 0.124 nm^2) of a hydrogen molecule, which were evaluated from the bulk liquid and solid densities, assuming the close packing of spheres (Table 1). The BET surface areas that were obtained from hydrogen adsorption using both of the cross-sectional areas (from the liquid and solid densities) are 44% and 26% larger than that from nitrogen adsorption, respectively. This is in good agreement with the results of the adsorption experiments on MCM-41 by Edler et al.[8] (40% and 14% deviations, respectively; they used 0.144 nm^2 and 0.117 nm^2 as the cross-sectional area of a hydrogen molecule, assuming the adsorbed liquid and solid hydrogen.). The large monolayer capacities of hydrogen for SWNHs and MCM-41 are anomalous because it indicates that adsorbed hydrogen in the first layer is greatly compressed compared with solid hydrogen in the bulk. However, such anomalous monolayer capacities have been also obtained when the BET theory is applied to helium adsorption isotherms below the normal boiling points. Steele attributed it to appreciably larger energy of an atom in the second layer than that in the bulk liquid and derived a modified BET equation[44]

$$\frac{n}{n_m} = 1 + \frac{zx}{(1-x)(1+zx-x)} \qquad (6)$$

where $x = P/P_0$, n is the adsorbed amount of gas, n_m is the adsorbed amount of gas in a monolayer, and z is an adjustable parameter given by

$$z = \frac{j_2}{j_{liq}}\exp\left[\frac{-(\epsilon_2 - \epsilon_{liq})}{kT}\right] \qquad (7)$$

where j_n is the molecular partition function of a molecule in the nth adsorbed layer, ϵ_n is the difference in zero point energy of an adsorbed molecule and that in the gas, the subscript liq denotes the bulk liquid. Note that the last term in eq 6 is formally the BET equation if the c constant in the BET theory is substituted for z. This modified BET equation corresponds to the adsorption system in which a monolayer formation occur at a negligibly small pressure, and a second BET-type layer is formed on the top of the monolayer. This adsorption system complete the first layer, which is achieved at a fairly low pressure, is in agreement with the prediction from the PIMC simulations for hydrogen adsorption on graphite at 20 K;[42] thus, Steele's modified BET equation should be applicable to the hydrogen adsorption inside SWNHs due to the discussion in the previous section. Huber and Huber applied this theory to hydrogen adsorption on Vycor glass (d = 6.3 nm) below 20 K and showed that a better fit to the adsorption data is obtained by Steele's modified BET equation. However, in the case of the inside of SWNHs, the amount adsorbed in the second layer should be lower than that in the first layer because of the packing

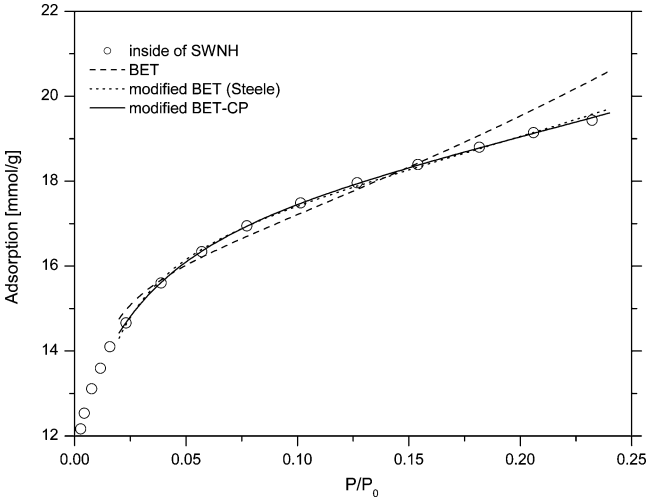

Figure 9. The fit of the theoretical isotherms (BET and modified BET theories) to the experimental adsorption isotherm of hydrogen for the inside of SWNHs at 20 K.

TABLE 2: Surface Areas from the Modified BET Equations for the Interior of SWNHs (Hydrogen Adsorption at 20 K)

	n_m[a] mmol/g	n_s[b] mmol/g	z[c]	S_{mBET}[d] m^2/g	P/P_0[e]	Δ[f] %
Steele	8.7		85	746[(l)g]	0.02−0.23	−20
				650[(s)g]		−31
this study	11.8	6.5	31	1021[(l)g]	0.02−0.23	8.5
				890[(s)g]		−5.4

[a] n_m denotes BET monolayer capacity. [b] n_s denotes second layer capacity. [c] z is adjustable parameter that correspondes to the heat of adsorption for second layer formation. [d] S_{mBET} denotes surface area. [e] P/P_0 refers to the range of least-squares fitting for BET analysis. [f] Δ denotes the difference from the surface area obtained by nitrogen adsorption (Table 1). [g] (*l*)(*s*) refer to surface areas estimated by use of the cross-sectional areas, which were calculated from the bulk liquid and solid (triple point) hydrogen densities by assuming the close packing of spheres.

constraint for the cylindrical geometry. Therefore, we introduced one more parameter to Steele's modified BET equation to take into account the geometrical packing constraint of a second layer in a cylindrical pore (denoted as modified BET-CP equation in this paper)

$$\frac{n - n_m}{n_s} = \frac{zx}{(1 - x)(1 + zx - x)} \tag{8}$$

where n_s is adsorbed amount of gas in a second layer. The least-squares fitting was performed so that eq 8 has the best fit with the hydrogen adsorption isotherm inside SWNHs at 20 K, and the result is shown in Figure 9 together with the results using BET and Steele's modified BET equations. The fit of the BET equation to the hydrogen adsorption data results in rather poor agreement above $P/P_0 = 0.15$. However, both eqs 6 and 8 give a fairly better fit than the BET equation over a wide range of relative pressures. The parameters obtained by the fit of the modified BET equations are listed in Table 2. The surface area of the interior of SWNHs can now be estimated by assuming the liquid and solid hydrogen densities. The surface areas obtained by Steele's model using both of the hydrogen densities are much smaller than that from the nitrogen adsorption, whereas the values calculated by the method proposed here agree fairly well with the surface area from the nitrogen data, especially when the solid hydrogen density is assumed (the deviation is ca. 5%). The value of $-(\epsilon_2 - \epsilon_{liq})$ can be calculated by eq 7 from the assumption that $j_2/j_{liq} = 1$, thus, $-(\epsilon_{2-}\epsilon_{liq})/k = 89$ K from Steele's model and $-(\epsilon_{2-}\epsilon_{liq})/k = 69$ K from the modified BET-CP model, respectively. Here, the quantum effective potential for hydrogen inside SWNT with $D = 3$ nm at 20 K is 59 K at the effective position of the second layer (σ_{ff}' away from the position of the maximum potential well depth, Figure 2). The potential value for the SWNT system roughly agrees with the predicted heat by our model. According to Steele,[44] the isosteric heat of adsorption in the second layer, $q_{st}^{(2)}$ can be written as

TABLE 3: Pore Volumes for the Interior of SWNHs

N_2 (77 K)	H_2 (20 K)	
V_p[a] cm^3/g	V_p[a] cm^3/g	Δ[b] %
0.55[(l)c]	0.63[(l)c]	15
	0.51[(s)c]	−6.3

[a] V_p denotes pore volume obtained from the adsorbed amount at $P/P_0 = 0.8$. [b] Δ denotes the difference from the pore volume obtained by nitrogen adsorption. [c] (*l*)(*s*) refer to the pore volumes estimated from the bulk liquid and solid (triple point) densities.

$$q_{st}^{(2)} = \Delta H_{vap} - (\epsilon_2 - \epsilon_{liq}) \tag{9}$$

where ΔH_{vap} is the enthalpy of vaporization. Daunt et al.[46] reported approximately 1.3 kJ/mol for $q_{st}^{(2)}$ in the second layer of hydrogen on the graphite at 20 K. The $q_{st}^{(2)}$ value estimated by eq 9 is 1.5 kJ/mol for our model, thus again good agreement is obtained, taking into account that the interaction potential of hydrogen inside small SWNTs would be stronger than that for the graphite basal plane.

As listed in Table 2, the n_s value obtained by the fitting of the modified BET-CP equation is 55% of the n_m value. For a system obeying the assumptions of the modified BET-CP model, the ratio of n_s to n_m should be relative to the ratio of the radius of the second layer film to that of the first layer film, if the densities in the two layers are equal to each other. Here, we assume that the radius of the cylindrical monolayer, r_m, corresponds to the position of the potential minimum calculated by the quantum solid−fluid effective potential for hydrogen inside the model SWNT (eq 2 with eq 1) that and the second layer is formed at $r_s = r_{m-}\sigma_{ff}'$. Calculated r_s/r_m values are 0.52 for SWNT with $D = 2$ nm (the effective diameter: $d = D - \sigma_{ss} = 1.66$ nm) and 0.72 for $D = 3$ nm ($d = 2.66$ nm), respectively. These are comparable with the n_s/n_m value obtained for the inside of SWNHs ($n_s/n_m = 0.55$). The diameters considered above should be reasonable because the average diameter of SWNHs is 2.3 nm by use of the nitrogen data and a relation of $d = 4\ V_p/S_{BET}$ and also from the TEM observations.[20]

Although our model would also suffer from the multilayer adsorption and capillary condensation complications inside SWNHs as predicted by nitrogen adsorption in the model SWNTs and discussed in the previous section, our analysis gives a reasonable agreement with the results from nitrogen adsorption, and it would suggest that the adsorbed hydrogen in the monolayer is compressed compared with the bulk liquid. Moreover, the results of this calculation indicate that the energy of a hydrogen molecule in the second layer is larger than that in the bulk liquid. This can be attributed to the fact that, although the fluid−fluid interaction of hydrogen in the liquid is fairly reduced by the quantum effects, the solid−fluid interaction can hardly be affected at the position of the second layer.

Confinement of Quantum Hydrogen inside SWNHs. The pore volume for the internal space of SWNHs in Table 3 that

was obtained from the adsorbed amount of hydrogen at $P/P_0 = 0.8$ by use of the bulk liquid density (35.1 mmol/cm^3) at the normal boiling temperature is 15% larger than that calculated from nitrogen isotherm using the liquid density in the bulk. However, if we assume that the confined hydrogen inside SWNHs has an average density of solid hydrogen (43.2 mmol/cm^3) in the bulk at the triple point, then good agreement with the value from the nitrogen data is obtained within 6.3% deviation. Moreover, if the density of the confined nitrogen inside SWNHs is approximately 7% larger than that of the bulk liquid as predicted by the DFT models, then the pore volumes from assumptions of solid hydrogen and enhanced liquid nitrogen densities are almost identical to each other. Therefore, we can deduce that the average density of confined hydrogen inside SWNHs is more densely packed than that in the free liquid and approaches the solid hydrogen density in agreement with the conclusions of the work by Edler and co-workers.[8] One possible reason for the enhanced density of the confined hydrogen inside SWNHs is that quantum effects, which are not significant for nitrogen, give a strongly attractive pore situation because the potential well depth of the fluid−fluid interaction of hydrogen can be more reduced by quantum effects than that of the fluid−wall interaction at 20 K. This is analogous to the argument[9,11] that the freezing point elevation of adsorbed classical LJ methane can be induced in the strongly attractive pores.

Conclusions

We have measured the adsorption isotherms of hydrogen and nitrogen on as-SWNH and ox-SWNH at 20 and 77 K, respectively, and the isotherms for the inside of SWNHs were obtained by subtraction of the isotherms on as-SWNH from those on ox-SWNH. Up to a relative pressure of ca. 0.5, the experimental isotherm of nitrogen inside SWNHs shows a gradual increase, indicating that the tube size distribution of SWNHs ranges to about 6 nm from the DFT calculations. The DFT models also predict that the average densities of confined nitrogen inside SWNTs ($D = 2-6$ nm) are only 4.4−7.1% larger than that of the bulk liquid at $P/P_0 = 0.8$. This suggests that the pore volume inside SWNHs can be evaluated using the density of liquid nitrogen within about 7% deviation, following the Gurvich rule.[47] Although the monolayer density of the adsorbed nitrogen from the DFT model is actually close to the $\rho_{2D-bulk}$ value in the intermediate relative pressure region, the BET surface area from nitrogen adsorption inside SWNHs would be strongly affected by the packing constraint of adsorbed nitrogen in the first layer for the cylindrical geometry because of the overestimation of the monolayer capacity due to the multilayer adsorption and capillary condensation over the relative pressure region, where the BET equation is usually fit.

The surface area from hydrogen adsorption using the BET theory is anomalously large compared with that for nitrogen; however, the modified BET-CP model, which is based on the assumptions that the energy of a hydrogen molecule in the second layer is larger than that in the liquid and that the second layer capacity is constricted because of the cylindrical geometry of SWNH, gives a reasonable surface area, especially when the adsorbed hydrogen in the first layer is assumed to be in a solidlike state. This suggests that the adsorbed hydrogen in the monolayer is compressed compared with liquid hydrogen.

The pore volume for the inside of SWNHs from the liquid hydrogen density is 15% larger than that calculated from the nitrogen data, whereas, assuming the solid hydrogen density, good agreement is obtained within 6% deviation. This indicates that the average density of confined hydrogen inside SWNHs is more densely packed than in the bulk liquid. This is in agreement with the conclusions of the work by Edler and co-workers.[8]

Our results for hydrogen are attributed to the quantum effects, which are negligible for nitrogen, that give a strongly attractive pore situation for hydrogen−SWNH system; that is, the potential well depth of the fluid−fluid interaction of hydrogen can be more reduced by the quantum effects than the fluid−wall interaction at 20 K. The difference comes from the fact that a pair of quantum hydrogen molecules can be regarded as two Gaussian packets in the Feynman−Hibbs picture due to the small mass of hydrogen, but carbon atoms in the wall of SWNH cannot because they are rigidly linked together, thus, the uncertainty in position of the carbon atoms does not contribute to the hydrogen−SWNH interaction.

Further work will be needed to study the properties of confined hydrogen inside SWNHs at low temperatures using the heat capacity and neutron scattering measurements and molecular simulations, including the quantum effects, to confirm the solidlike structure of adsorbed hydrogen.

Acknowledgment. This work was partially funded by Grand-in-Aid for Fundamental Scientific Research (S) (no. 15101003) from the Japanese Government and the Advanced Nanocarbon Application Project, NEDO.

References and Notes

(1) Tell, J. L.; Maris, H. J. *Phys. Rev. B* **1983**, *28*, 5122.
(2) Torii, R. H.; Maris, H. J.; Seidel, G. M. *Phys. Rev. B* **1990**, *41*, 7167.
(3) Sokol, P. E.; Azuah, R. T.; Gibbs, M. R.; Bennington S. M. *J. Low Temp. Phys.* **1996**, *103*, 23.
(4) Stan, G.; Cole, M. W. *J. Low Temp. Phys.* **1998**, *112*, 539.
(5) Wilson, T.; Tyburski, A.; DePies, M. R.; Vilches, O. E.; Becquet, D.; Bienfait, M. *J. Low Temp. Phys.* **2002**, *126*, 403.
(6) Tanaka, H.; Murata, K.; Miyawaki, J.; Kaneko, K.; Kokai, F.; Takahashi, K.; Kasuya, D.; Yudasaka, M.; Iijima, S. *Mol. Cryst. Liq. Cryst.* **2002**, *388*, 429.
(7) Ginzburg, V. L.; Sobyanin, A. A. *Sov. Phys. JETP Lett.* **1972**, *15*, 242.
(8) Edler, K. J.; Reynolds, P. A.; Branton, P. J.; Trouw, F. R.; White, J. W. *J. Chem. Soc., Faraday Trans.* **1997**, *93*, 1667.
(9) Miyahara, M.; Gubbins, K. E. *J. Chem. Phys.* **1997**, *106*, 2865.
(10) Watanabe, A.; Iiyama, T.: Kaneko, K. *Chem. Phys. Lett.* **1999**, *305*, 71.
(11) Maddox, M. W.; Gubbins, K. E. *J. Chem. Phys.* **1997**, *107*, 9659.
(12) Wang, Q.; Johnson, J. K. *J. Chem. Phys.* **1999**, *110*, 577.
(13) Wang, Q.; Challa, S. R.; Sholl, D. S.; Johnson, J. K. *Phys. Rev. Lett.* **1999**, *82*, 956.
(14) Challa, S. R.; Sholl, D. S.; Johnson, J. K. *Phys. Rev. B* **2001**, *63*, 245419.
(15) Challa, S. R.; Sholl, D. S.; Johnson, J. K. *J. Chem. Phys.* **2002**, *116*, 814.
(16) Levesque, D.; Gicquel, A.; Darkrim, F. L.; Kayiran, S. B. *J. Phys.: Condens. Matter* **2002**, *14*, 9285.
(17) Gu, C.; Gao, G. H. *Phys. Chem. Chem. Phys.* **2002**, *4*, 4700.
(18) Gu, C.; Gao, G. H.; Yu, Y. X. *J. Chem. Phys.* **2003**, *119*, 488.
(19) Harris, P. J. F.; Tsang, S. C.; Claridge, J. B.; Green, M. L. M. *J. Chem. Soc., Faraday Trans.* **1994**, *90*, 2799.
(20) Iijima, S.; Yudasaka, M.; Yamada R.; Bandow, S.; Suenaga, K.; Kokai, F.; Takahashi, K. *Chem. Phys. Lett.* **1999**, *309*, 165.
(21) Murata, K.; Kaneko, K.; Kokai, F.; Takahashi, K.; Yudasaka, M.; Iijima, S. *Chem. Phys. Lett.* **2000**, *331*, 14.
(22) Murata, K.; Kaneko, K.; Steele W. A.; Kokai, F.; Takahashi, K.; Kasuya, D.; Yudasaka, M.; Iijima, S. *Nano Lett.* **2001**, *4*, 197.
(23) Ohba, T.; Murata, K.; Kaneko, K.; Steele W. A.; Kokai, F.; Takahashi, K.; Kasuya, D.; Yudasaka, M.; Iijima, S. *Nano Lett.* **2001**, *7*, 371.
(24) Murata, K.; Kaneko, K.; Steele W. A.; Kokai, F.; Takahashi, K.; Kasuya, D.; Hirahara, K.; Yudasaka, M.; Iijima, S. *J. Phys. Chem. B* **2001**, *105*, 10210.
(25) Bekyarova, E.; Hanzawa, Y.; Kaneko, K.; Silvestre-Albero, J.; Sepulveda-Escribano, A.; Rodriguez-Reinoso, F.; Kasuya, D.; Yudasaka, M.; Iijima, S. *Chem. Phys. Lett.* **2002**, *366*, 463.

(26) Murata, K.; Kaneko, K.; Kanoh, H.; Kasuya, D.; Takahashi, K.; Kokai, F.; Yudasaka, M.; Iijima, S. *J. Phys. Chem. B* **2002**, *106*, 11132.
(27) Takaishi, T.; Sensui, Y. *Trans. Faraday Soc*. **1963**, *53*, 2503.
(28) Tjatjouls, G. J.; Feke, D. L.; Mann, J. A., Jr. *J. Phys. Chem.* **1988**, *92*, 4006.
(29) Tanaka, H.; El-Merraoui, M.; Steele, W. A.; Kaneko, K. *Chem. Phys. Lett.* **2002**, *352*, 334.
(30) Ravikovitch, P. I.; Haller, G. L.; Neimark, A. V. *Adv. Colloid Interface Sci.* **1998**, *76*−*77*, 203.
(31) Feynman, R. P. *Statistical Mechanics*; Benjamin: Reading, MA, 1972.
(32) Young, R. A. *Phys. Rev. Lett*., **1980**, *45*, 638.
(33) Neimark, A. V.; Ravikovitch, P. I.; Vishnyakov, A. *Phys. Rev. E* **2000**, *62*, 1493.
(34) Evans, R. In *Inhomogeneous Fluids*; Henderson, D., Ed.; Marcel Dekker: New York, 1992.
(35) Tarazona, P. *Phys. Rev. A* **1985**, *31*, 2672; **1985**, *32*, 3148.
(36) Weeks, J. D.; Chandler, D. Andersen, H. C. *J. Chem. Phys*. **1971**, *54*, 5237.
(37) Ravikovitch, P. I.; Vishnyakov, A.; Neimark, A. V. *Rhys. Rev. E* **2001**, *64*, 11602.
(38) Iiyama, T.; Nishikawa, K.; Otowa, T.; Kaneko, K. *J. Phys. Chem*. **1995**, *99*, 10075.
(39) Iiyama, T.; Nishikawa, K.; Suzuki, T.; Otowa, T.; Hijiriyama, M.; Nojima, Y.; Kaneko, K. *J. Phys. Chem. B*, **1997**, *101*, 3037.
(40) Ohkubo, T.; Iiyama, T.; Nishikawa, K.; Suzuki, T.; Kaneko, K. *J. Phys. Chem. B*, **1999**, *103*, 1859.
(41) Ohba, T.; Kanoh, H.; Kaneko, K. *J. Am. Chem. Soc*. **2004**, *126*, 1560.
(42) Wang, Q.; Johnson J. K. *Mol. Phys*. **1998**, *95*, 299.
(43) Ohba, T.; Kaneko, K. *J. Phys. Chem. B* **2002**, *106*, 7171.
(44) Steele, W. A. *J. Chem. Phys*. **1956**, *25*, 819.
(45) Huber, T. E.; Huber, C. A. *J. Low Temp. Phys*. **1990**, *80*, 315.
(46) Daunt, J. G.; Hedge, S. G.; Tsui, S. P.; Lerner, E. *J. Low Temp. Phys*. **1992**, *88*, 421.
(47) Rouquerol, F.; Rouquerol, J.; Sing, K. S. W. *Adsorption by Powders and Porous Solids*; Academic: San Diego, CA, 1999.